AIAA 2016-3848
AIAA Aviation
13-17 June 2016, Washington, D.C.
AIAA Atmospheric Flight Mechanics Conference

Towards Three-Dimensional Global Stability Analysis of Transonic Shock Buffet

Sebastian Timme* and Reik Thormann†
University of Liverpool, Liverpool, England L69 3GH, United Kingdom

A numerical study of the flow over a half wing-body configuration representative of a large civil aircraft is presented. In particular, we are interested in predicting the onset of the shock buffet instability. Reynolds-averaged Navier-Stokes simulations using the one-equation Spalart-Allmaras turbulence model are considered. First, forced-motion, time-linearised analysis is performed to investigate the frequency response behaviour of aerodynamic coefficients while approaching the buffet onset angle of attack. Secondly, global stability analysis with three inhomogeneous spatial directions is achieved for this realistic aircraft configuration in transonic turbulent flow with strong shock waves and boundary layer separation. The implicitly restarted Arnoldi method is applied, in conjunction with an advanced sparse iterative linear equation solver and an industrial computational fluids dynamics package, to calculate few eigenvalues of the complete fluid Jacobian matrix close to the origin of the complex plane for flow conditions near shock buffet onset.

I. Introduction

The work presents the details of a study to investigate the onset of shock buffet unsteadiness. Shock buffet is a phenomenon characterised by a strong interaction between the shock wave formed around a wing in transonic flow and the wing's turbulent boundary layer causing large-scale oscillatory shock motion. While the unsteadiness is self-excited and self-sustained without structural vibration, the resulting unsteady aerodynamic loads can excite the wing structure. As a consequence shock buffet limits the flight envelop of civil aircraft in the transonic range. This phenomenon has thus been studied intensively.

The unsteadiness can be observed in both two- and three-dimensional configurations. While the two-dimensional aerofoil case is characterised by harmonic shock motion at a distinct frequency, the behaviour in three dimensions, such as configurations representative of civil aircraft, is less clear. It is often reported that shock buffet on swept wing configurations is characterised by smaller shock movements with a larger frequency band.[1,2] Results of a recent study on a half wing-body configuration indicate that the onset of shock buffet can occur at a distinct frequency, while broadband unsteadiness develops with increasing distance from the onset conditions.[3,4] Close to onset conditions the unsteadiness is very localised, and corresponding time histories of quantities such as the lift coefficient indicate periodic motions.

The occurrence of distinct frequencies in the unsteady signal could indicate that the onset of the three-dimensional shock buffet phenomenon follows the mechanism of a Hopf bifurcation, similar to studies on two-dimensional aerofoils, where a pair of complex conjugate eigenvalues crosses the imaginary axis for a critical parameter value such as Mach number or angle of attack. Such stability analyses have shown a strong link between the appearance of shock unsteadiness and the presence of an unstable global mode.[5–8] A critical value of the angle of attack exists above which the shock starts to oscillate. In a similar fashion, it was previously attempted to not only estimate the frequency and damping behaviour of a destabilising global mode from the corresponding eigenvalue, but also to predict the critical parameter value itself using the inexact Lyapunov inverse iteration method.[9,10] Importantly, no prior knowledge of a frequency shift close to the target eigenvalue is required, thus making the approach truely predictive. While simulations of flutter onset and also fluid-only instability, in the form of a laminar circular cylinder flow, were successful, numerical difficulties prevented the prediction of the aerofoil buffet onset.

*Lecturer, School of Engineering; sebastian.timme@liverpool.ac.uk.
†Research Associate, School of Engineering; reik.thormann@liverpool.ac.uk

Previous studies of buffeting aerofoils using global stability analysis applied sparse direct linear equation solvers with the coefficient matrix factorised in lower and upper triangular matrices and subsequent solution of resulting triangular systems. Excessive memory requirements are already observed for simple aerofoil cases. Indeed, when attempting to extrude an aerofoil into the spanwise direction to create a protoype three-dimensional wing, the memory requirements, even for a small case with only 300,000 grid points, reached 1.8 TB.[8] This will make such direct solution methods, when solving the linear systems resulting from a shift and invert approach such as employed in ARPACK,[11,12] infeasible for truly three-dimensional cases. An alternative method are sparse iterative linear equation solvers, such as the widely-used generalized minimal residual method (GMRES).[13] Such approaches however often fail to converge for very stiff problems, such as shifted linear systems arising in transonic turbulent flow near buffet onset.

This paper will discuss the challenges outlined above. Most importantly, it is attempted to identify the three-dimensional buffet onset behaviour from a global stability approach by using an advanced sparse iterative linear equation solver with deflated restarting, while combining ARPACK and the industrial computational fluid dynamics (CFD) code DLR-TAU.

II. Numerical setup

Test case

The test case is a half wing-body configuration scaled to wind tunnel dimensions. The semi-span of the model is 1.10 m, while the aerodynamic mean chord is about 0.279 m. The local chord lengths corresponding to the centre line and wing tip are 0.592 m and 0.099 m, respectively. The wing is twisted, tapered and has a constant sweep angle of 25 deg. This configuration has recently been investigated in the transonic wind tunnel facility of the Aircraft Research Association in the United Kingdom.

The simulations are set up to reproduce the aerodynamic field of the related wind tunnel tests, details of which are not further discussed in this work and the reader is referred to [14]. The Mach number is 0.8 while the Reynolds number (based on the aerodynamic mean chord) is 3.75 million. The reference temperature and pressure are 266.5 K and 66.0 kPa, respectively. Different to the experimental study and previous work, in which a laminar to turbulent transition is imposed near the wing leading edge, fully turbulent flow is assumed in the current study to avoid unnecessary additional uncertainty when forming the fluid Jacobian matrix for fixed transition. Far-field conditions are applied at a distance corresponding to 25 times the semi-span of the model (around 90 aerodynamic mean chords). Symmetry boundary condition is applied along the centre plane.

Grid

The unstructured mesh was produced using the Solar grid generator.[15] The meshing follows industry-accepted guidelines. For instance, the initial spacing normal to all viscous walls is less than 0.8 wall units for this coarse mesh, while the growth rate of cell sizes in the viscous layer is less than 1.3. The blunt trailing edge is described by 8 cells corresponding to a spacing of about 0.15% of the local chord. Concerning the span-wise mesh distribution, a spacing of 0.5% and 0.1% of the span is imposed for the wing root and tip, respectively. Altogether, the grid is composed of 2.7 million points corresponding to 4.7 million elements of mixed type including 12,000 prisms, 71,000 pyramids, 2.4 million hexahedral and 2.3 million tetrahedral elements. The grid spacing on the wing surface is presented in Figure 1a.

Nonlinear and time-linearised flow solver

The simulations were performed using the unstructured finite-volume solver TAU, developed by the German Aerospace Center (DLR) and widely used in the European aerospace sector, both in industry and academia. The Jameson-Schmidt-Turkel second-order central scheme with scalar artificial dissipation was applied to evaluate the inviscid fluxes of the mean flow equations, while the turbulence model, namely the Spalart-Allmaras (SA) model,[16] was discretised using a first-order upwind scheme. Gradients of the flow variables, used for the viscous and source terms, are reconstructed using the Green-Gauss theorem without further approximations. Convergence of the nonlinear flow equations to steady state is accelerated using local time-stepping and an implicit backward Euler solver with Lower-Upper Symmetric Gauss-Seidel iterations. Multigrid is not applied in the current study.

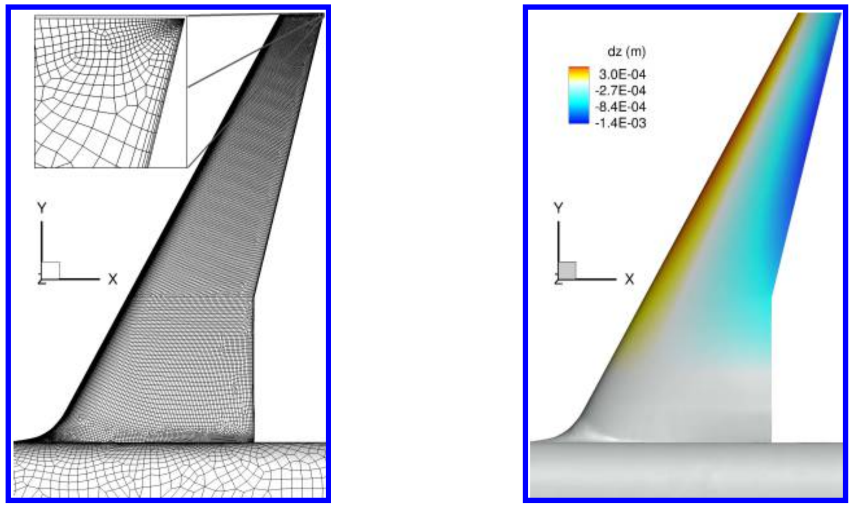

(a) Surface mesh

(b) Sythetic torsion mode

Figure 1. Surface point distribution and flexible synthetic mode projected onto surface mesh.

For time-dependent computations, both fluid-only on rigid aircraft and forced response of flexible wing, the standard dual time-stepping approach is employed. A dynamic Cauchy convergence criterion is applied for iterations in dual time. Each time step is iterated until the drag coefficient, chosen as control variable, shows a relative error smaller than 10^{-8} within the last 20 inner iterations. A minimum of 50 inner iterations is always performed, regardless of the drag convergence, while the maximum number is limited to 500 iterations when the dynamic convergence control fails.

For linearised frequency-domain, also called time-linearised, computations, DLR-TAU follows a first-disretise-then-linearise, matrix-forming approach. When solving the resulting linear systems, an advanced linear equation solver combined with an incomplete lower-upper (ILU) factorisation for preconditioning is chosen to overcome non-converging solutions using the restarted GMRES solver. The advanced iterative solver is referred to as generalized conjugate residual solver with deflated restarting (GCRO-DR). Here an invariant Krylov subspace is recycled both between restarts when solving a single linear frequency-domain problem and for a sequence of equations when, in the current work, varying the right-hand side forcing term and diagonally shifting the Jacobian matrix. Details of the theory and implementation in the DLR-TAU code as well as application to aeroelastic problems can be found in [17]. Preconditioning is applied in the form of a local, block ILU factorisation where the coefficient matrix, used for the factorisation, is blended between matrices arising from a first- and second-order spatial discretisation.[18]

For the calculation of eigenvalues and corresponding eigenvectors in the global stability approach, the implicitly restarted Arnoldi method as realised in the ARPACK library[11] is implemented within the DLR-TAU solver. This allows the exploitation of the CFD code's parallel infrastructure as well as its time-linearised solver functionality as described in the previous paragraph. Shift and invert spectral transformation is applied to achieve convergence to desired parts of the eigenspectrum, and therefore the solution of many linear systems is required as well with varying right-hand side terms.

Implementation and proper functioning of the time-linearised tools in the DLR-TAU code have previously been tested,[17,19,20] while coupling with the parallel ARPACK library[12] to extract few eigenvalues has been thoroughly investigated using the well-known low-Reynolds number instability on a circular cylinder as well as a buffeting aerofoil, results of which are not shown.

III. Moving towards frequency domain and global stability problem

First, we shortly present some results of nonlinear time-dependent simulations as reference to identify the shock buffet onset using a conventional approach. Secondly, forced-response calculations of a two-dimensional NACA0010 aerofoil are discussed as an analogy while quickly moving on to the half wing-body configuration

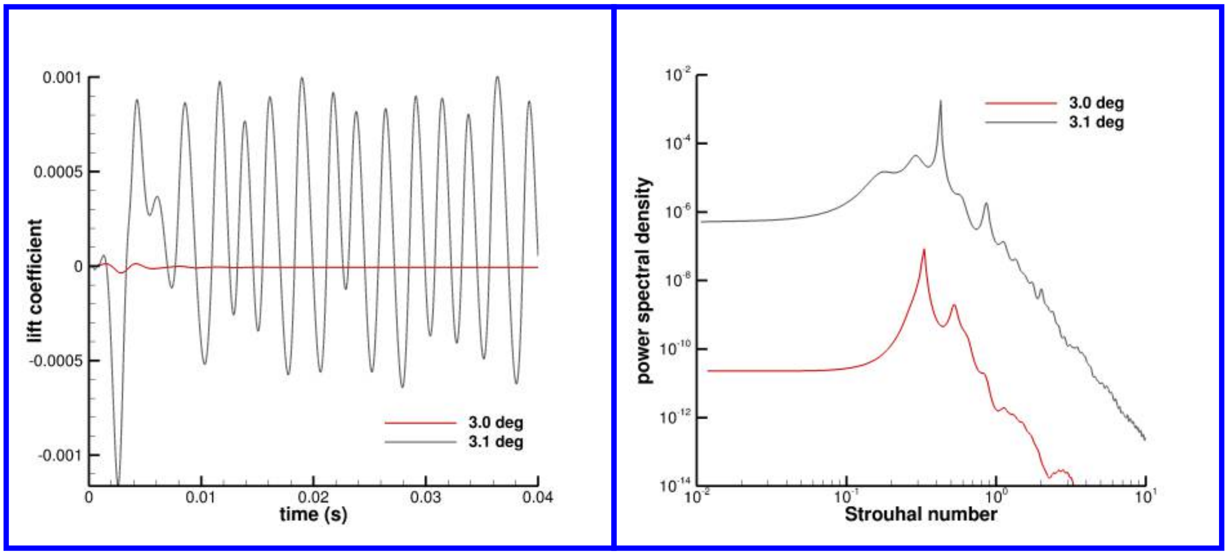

(a) Time history

(b) Power spectral density

Figure 2. Time history and corresponding power spectral density of lift coefficient around buffet onset.

trying to identify resonant behaviour which could indicate the presence of a lightly damped mode. Finally, we investigate the extraction of eigenvalues for the three-dimensional configuration near the buffet onset to discuss global linear stability, compare with the forced motion results, and analyse the observations for a possible instability mechanism.

Nonlinear, time-dependent simulations

Following the steady-state simulations, Figure 2a shows time histories of the lift coefficient for the half wing-body configuration just below buffet onset at 3.0 deg angle of attack and above at 3.1 deg. At the lower angle of attack, using an imperfectly converged steady solution as initial disturbance, the unsteady response quickly decays, while for the buffet condition the unsteady signal persists without additional excitation. Decreasing the increment in angle of attack even further and running additional simulations not reported herein, the buffet onset is found at about 3.03 deg.

Figure 2b compares the corresponding power spectral densities of the lift coefficient. For the angle of attack just above the onset of self-sustained instability, a rather distinct peak can be observed at a Strouhal number (based on the aerodynamic mean chord) of about 0.4, corresponding to 400 Hz. This frequency can indeed be found by simply counting the buffet cycles in the time history. The signals, both below and above the buffet onset, indicate in addition a stronger frequency content for Strouhal numbers between about 0.1 and 0.8 corresponding to 100 and 800 Hz. This range should be kept in mind in the following discussion. Interestingly, Strouhal numbers from 0.2 to 0.6 were recently reported for developed buffet on three-dimensional wings.[21]

Time-linearised, forced-response calculations

For two-dimensional aerofoils, there is evidence that buffet can be treated as a linear stability problem, i.e. the instability is linked to an unstable global mode. The eigenvalues of the fluid Jacobian matrix change with respect to a bifurcation parameter, e.g. Mach number or angle of attack. One of the many eigenvalues eventually crosses the imaginary axis and the flow becomes unstable.[5–8] If an eigenvalue is close to the imaginary axis (still stable however) and the flow is excited at the corresponding frequency, such as a pitching motion, resonant behaviour can be observed in quantities such as aerodynamic derivatives. A distinct peak is found in the frequency response function. The response peak is more and more pronounced,

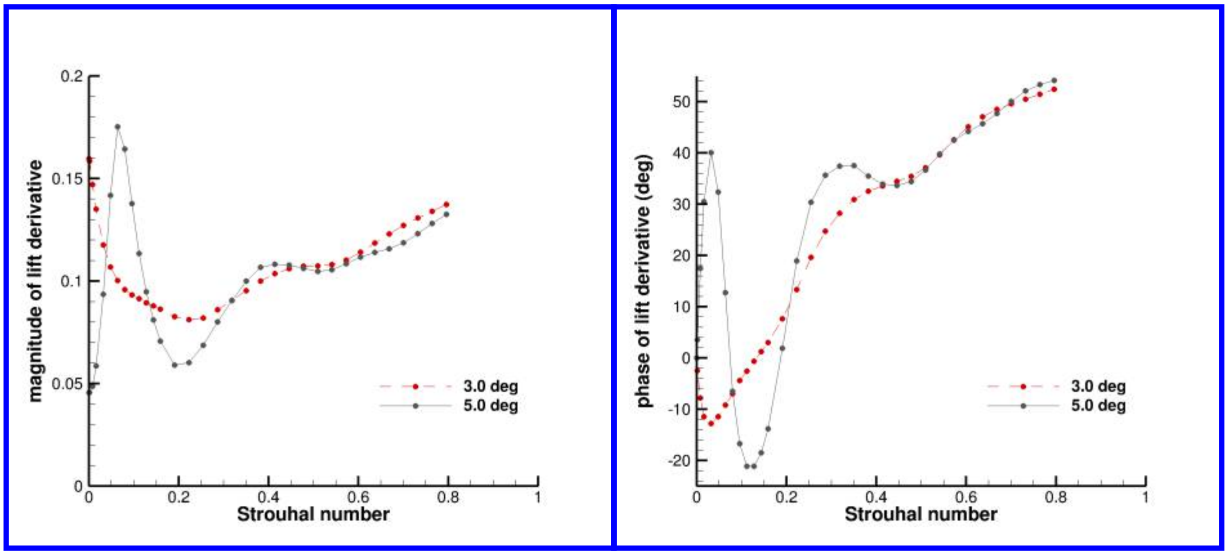

(a) lift magnitude

(b) lift phase in deg

Figure 3. Frequency response of lift coefficient for NACA0010 aerofoil.

while the eigenvalue approaches the imaginary axis. It was shown for a BAC311 profile that the location of the resonance peak is independent from the mode of excitation.[22] Similar results were presented for a NACA0012 aerofoil.[23] The corresponding phase exhibits an inflection point at the resonance frequency in addition to a change of sign.

Linearised frequency-domain methods can be applied as demonstrated for a NACA0010 aerofoil.[24] The linear system of equations arising from the linearised aerodynamics are very stiff near the buffet onset, resulting in situations where the problem does not converged with standard solution methods. More advanced solution techniques are hence required to converge the linear system at all frequencies. In Figure 3, an ILU-preconditioned GMRES iterative solver was applied to the same test case and convergence was achieved even close to the resonance frequency. At 3.0 deg angle of attack, the flow is attached and the frequency response due to a quarter-chord pitching motion shows qualitively the same behaviour as predicted by linear potential theory. The response function at an angle of attack of 5.0 deg, close to buffet onset, exhibits the resonance peak in the magnitude as well as the inflection point in the phase, similar to the time-domain results presented previously.[24] It is interesting to note that the Strouhal number for the resonance peak is at about 0.06 to 0.07, as recently reported in [21].

However, two levels of fill-in for the ILU factorisation as well as a relatively large number of Krylov vectors are required to achieve convergence. This significantly increases the computational cost, and becomes prohibitive for large three-dimensional cases as discussed in this work. While for small two-dimensional cases such consideration can be overcome with a "bigger" computer, using even direct linear equation solvers, for industry-relevant cases with many million grid points it exceeds the limits of common, currently available computer clusters. An example is presented in Figure 4a showing the memory requirements of direct and iterative linear solvers as a function of number of grid points. While the lower two data points obtained for a direct solver are from two-dimensional cases using the SuperLU sparse direct solver library,[25] the data points for the three-dimensional configuration (actually an aerofoil extruded in spanwise direction) are taken from [8]. The MUMPS library[26] was employed in that work instead. The biggest reported case consisted of about 300,000 grid points. The smallest grid available for the current buffet case has 2.7 million points. Extrapolation of available data gives memory requirements three to four orders of magnitude higher than an iterative solver with zero-fill-in ILU preconditioning. Of course, depending on the ordering strategy for the lower-upper factorisation of the direct solver, the memory requirements can vary. The estimated 100 to 1000 TB of memory for a relatively small mesh is not feasible regardless. Alternative solution approaches must be sought instead.

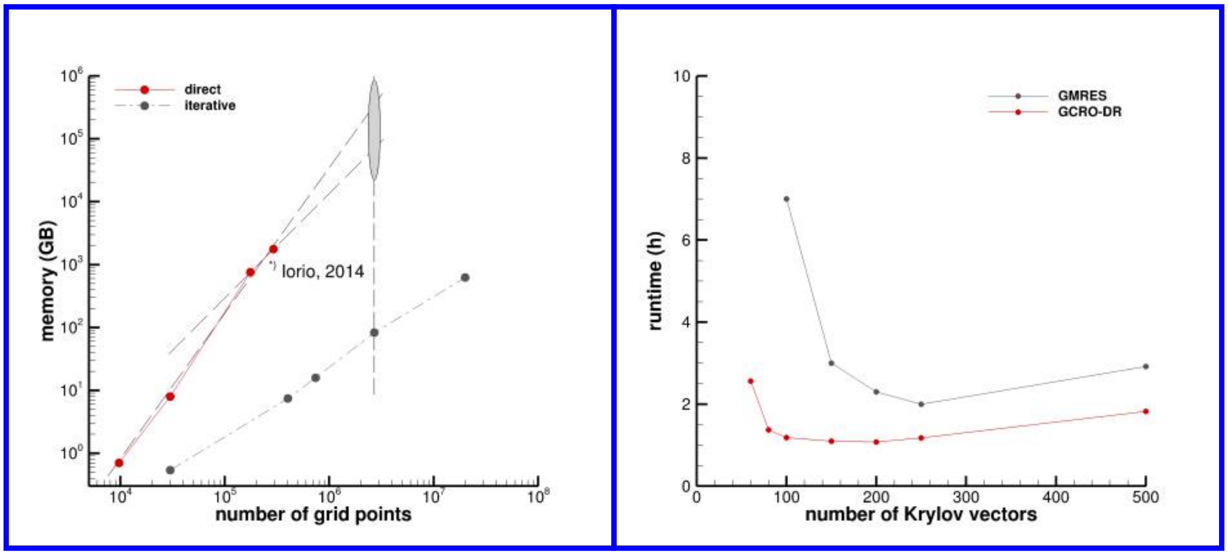

(a) memory requirements of linear equation solvers

(b) performance of iterative solvers at 2.8 deg angle of attack to achieve ten orders of magnitude convergence

Figure 4. Sparse direct and iterative linear solvers.

As outlined above in Sect. II, an advanced iterative linear equation solver, referred to as GCRO-DR, has recently been implemented in DLR-TAU and tested for aeroelastic applications with linearised aerodynamics arising from CFD.[17] A standard GMRES solver is prone to stall for very stiff problems, which would results in more levels of fill-in for ILU preconditioning and/or more Krylov vectors. In addition, iterative solvers are usually restarted to limit the memory requirements aggravating the issue of stalling. The new solver achieves faster convergence with less memory requirements as shown in Figure 4b presenting results for the half wing-body configuration in pre-buffet at an angle of attack of 2.8 deg. The data points represent a convergence of ten orders of magnitude for the time-linearised system following the calculation of a steady-state solution. The advantages over standard GMRES are clearly visible. Significant computational savings can be achieved.

Figure 5 presents magnitude and phase of the dynamic derivative of the lift coefficient following a frequency sweep at four angles of attack. The system was excited using a synthetic flexible torsion mode, as shown in Figure 1b. All simulations were run in about one to two hours on 72 cores while not exceeding 100 GB memory in total. Interestingly, the wing seems to exhibit similar behaviour to the aerofoil case discussed above when moving from 2.0 deg to 2.9 deg angle of attack. For the higher angles of attack, a rather distinct resonant peak is formed centred at a Strouhal number of about 0.11, while the aerodynamic response leads the structural excitation in phase in the frequency range, where the magnitude approaches its local maximum with increasing frequency. This behaviour could indicate the presence of a destabilising global mode similar to the two-dimensional case. Increasing the angle of attack even further to 3.0 deg and above, with the buffet onset being imminent, an unusual response behaviour at Strouhal numbers between 0.3 and 0.7, beyond the primary resonant peak, is observed. Slightly incrementing the angle of attack further to 3.01 deg, it can be observed that the primary peak does not exhibit a high sensitivity, while the higher-frequency behaviour seems to be strongly amplified. These results could indicate the presence of additional destabilising modes.

To cross-check the frequency-domain predictions, a forced-response time-domain simulation was performed as well at 3.0 deg angle of attack. The results together with the corresponding frequency-domain data are presented in Figure 6. The system is excited with the same synthetic flexible mode using a skewed pulse signal in the modal amplitude to cover the entire frequency range of interest at once. All required detail of such pulse excitations can be found in [27]. The frequency-domain prediction is accurate compared to the time-domain results confirming the above observations.

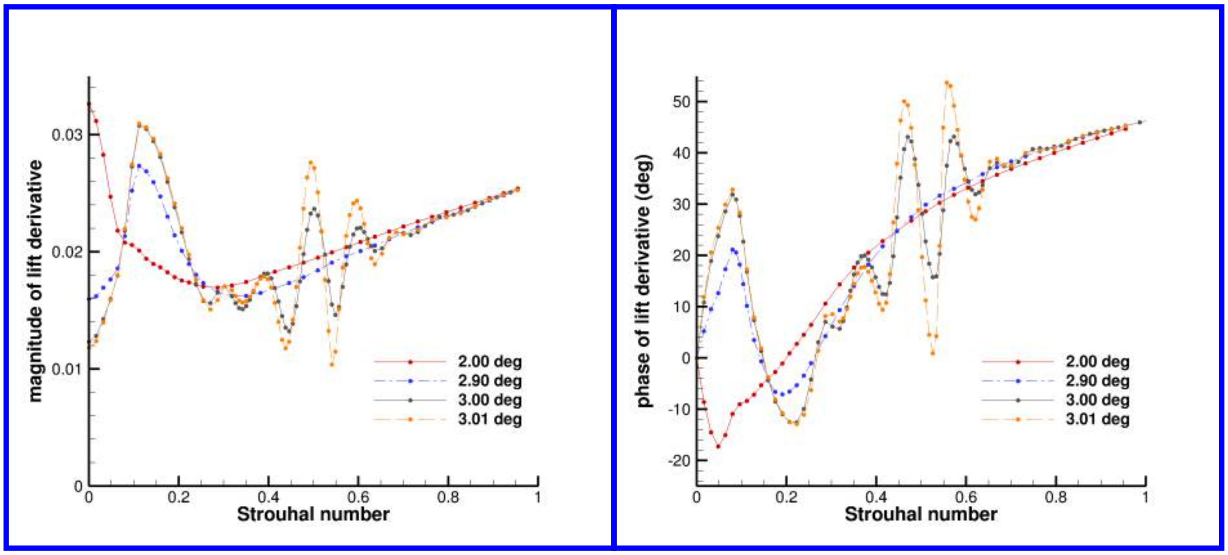

(a) lift magnitude

(b) lift phase in deg

Figure 5. Frequency response of lift coefficient due to flexible torsion mode.

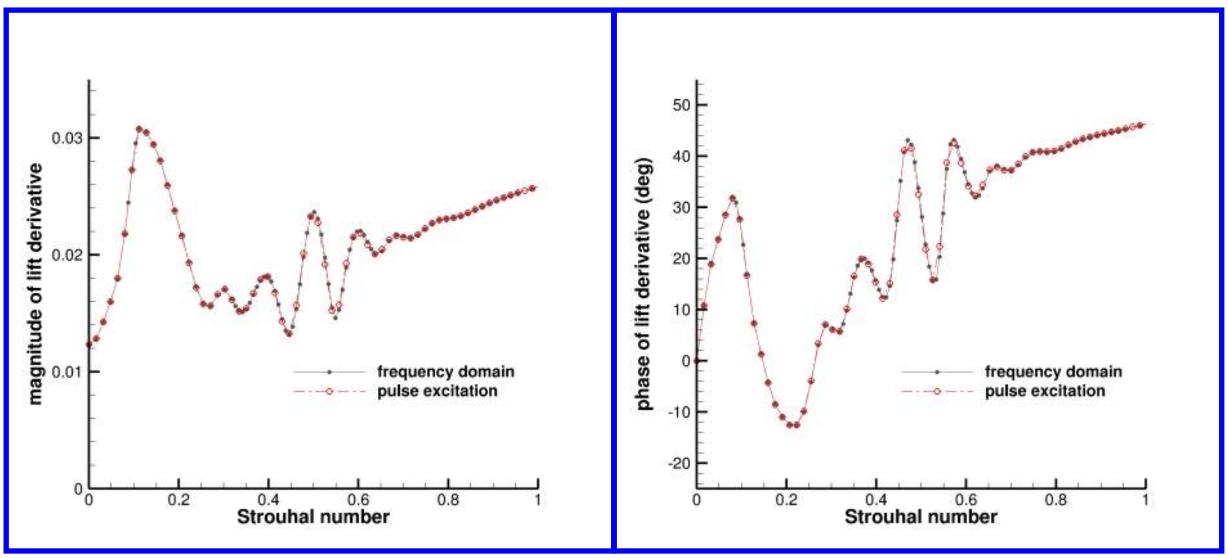

(a) lift magnitude

(b) lift phase in deg

Figure 6. Frequency response of lift coefficient due to flexible torsion mode and corresponding results from pulse excitation at 3.0 deg angle of attack.

Several magnitude plots of the complex-valued unsteady surface pressure distribution are provided in Figures 7 and 8. Results are shown for three angles of attack focusing on the two Strouhal numbers of 0.11 (first resonance peak) and 0.51 (dominant higher-frequency peak). The behaviour at the first resonance peak shown in Figure 7 indicates an unsteady shock foot in a wider part along the span increasing in intensity with increasing angle of attack. Downstream of the shock foot, lower-level unsteadiness can be observed as well. The unsteady characteristics change in the higher-frequency region as presented in Figure 8. Here for

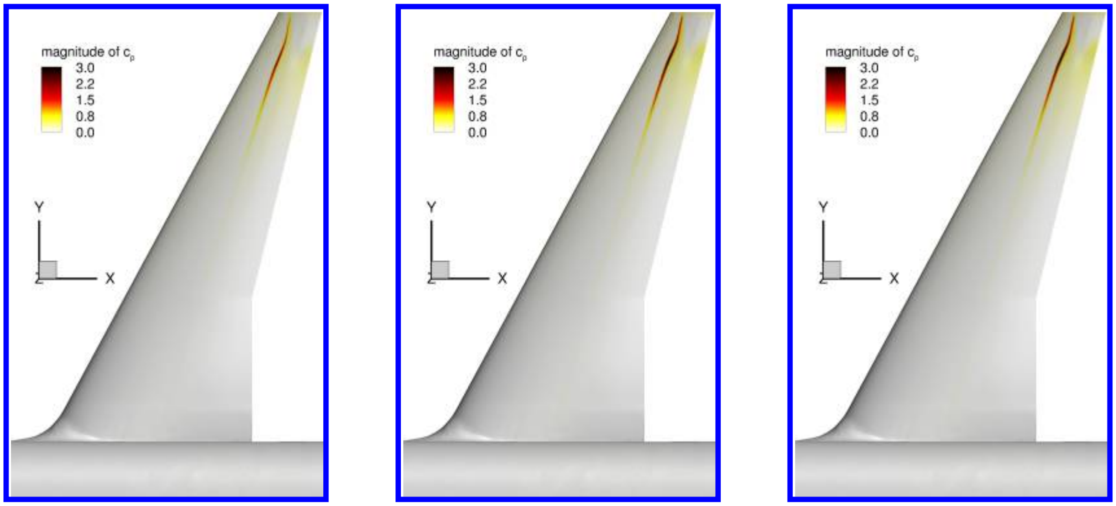

(a) 2.9 deg (b) 3.0 deg (c) 3.01 deg

Figure 7. Magnitude of derivative of surface pressure coefficient at lower-frequency dominant peak with Strouhal number of 0.11.

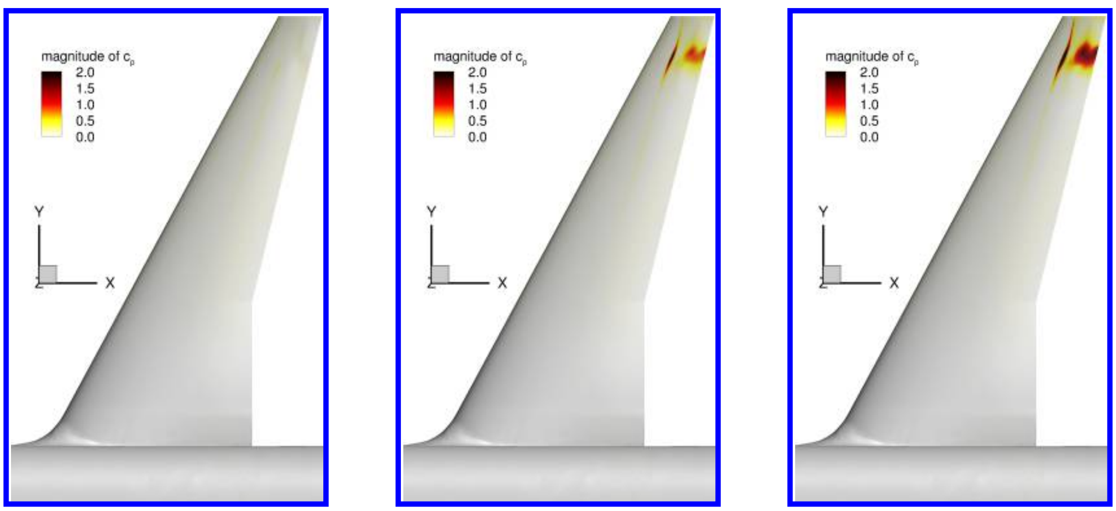

(a) 2.9 deg (b) 3.0 deg (c) 3.01 deg

Figure 8. Magnitude of derivative of surface pressure coefficient around higher-frequency peaks at Strouhal number of 0.51.

the two higher angles of attack, the spanwise extent of the unsteady shock foot is reduced and concentrated more towards the wing tip. In addition, a strong response is now also found downstream of the shock foot. The distinct spatial pattern could indicate a different physical mechanism. Interestingly, the same region of increased pressure perturbation found for the higher-frequency excitation is also observed in the statistics of the unsteady time-domain data, corresponding to Figure 2, as given by the pressure standard deviation. Finally, corresponding to a lack of resonant behaviour in the lift derivative in Figure 5, a distinct unsteadiness is not observed for 2.9 deg angle of attack either. These observations are further analysed in the next section focusing on eigensolutions.

A final point should be made when comparing the forced excitation with the time-dependent simulation results shown in Figure 2. Specifically, while the interesting higher-frequency behaviour can also be observed

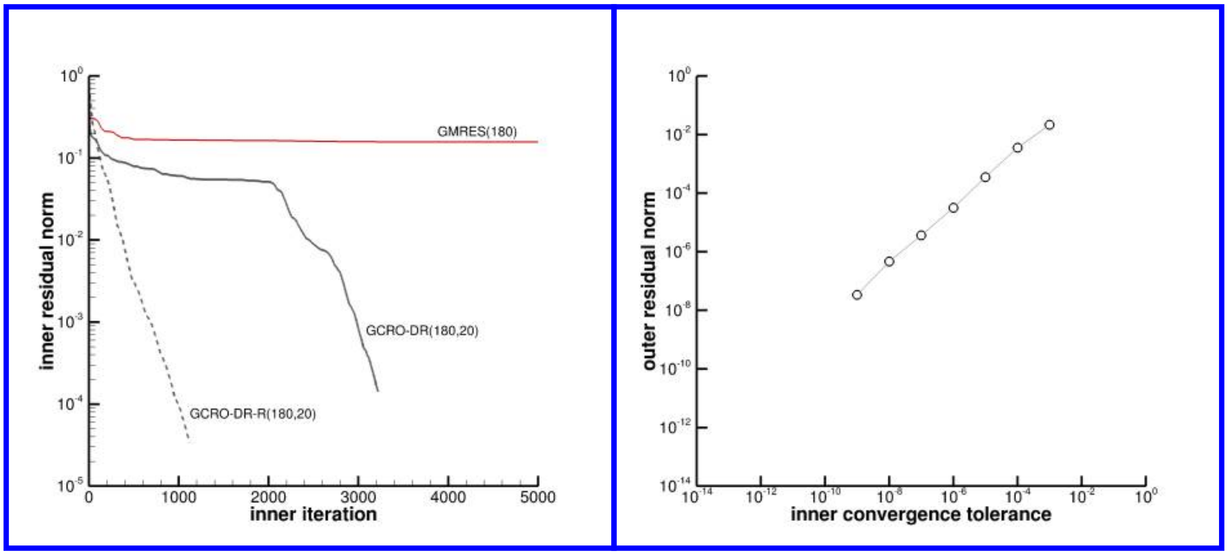

(a) typical convergence behaviour of linear solvers

(b) relation between inner and outer convergence

Figure 9. Convergence of inner-outer system at angle of attack of 3.0 deg and shift $\sigma = 3.0i$.

in the power spectral density of the lift coefficient at 3.0 deg angle of attack, the lower-frequency resonance is not noticed. Different forms of excitation should be applied to make sure that all relevant frequencies are covered. It could be that an initial disturbance based on an imperfectly converged steady solution does only excite the higher-frequency phenomenon. This indeed would make sense when arguing that this higher-frequency phenomenon kicks off the buffet instability, and is thus least damped and last to fully converge in a steady simulation.

Eigenvalue calculations

To calculate few eigenvalues and corresponding eigenvectors, the implicitly restarted Arnoldi method using the ARPACK library is applied. The shift and invert spectral transformation mode is required to calculate eigenvalues close to a desired, user-defined, complex-valued shift. The methods we describe are able to compute eigenvalues, for the first time in the authors' knowledge, of a three-dimensional, industry-relevant configuration in transonic turbulent flow. Indeed, we are able to extract eigenvalues around buffet onset conditions for a problem of dimension 16.3 million. All simulations were run on 72 cores using the same linear solver settings as for the forced-response calculations, while never exceeding a memory consumption of 125 GB in total (now including ARPACK's data storage). We swept along the imaginary axis, using several shifts consecutively, trying to identify eigenvalues approaching the axis. The increment in frequency shift was chosen so that the search regions overlap to increase confidence in not missing eigenvalues.

While shift and invert methods are rather powerful, they require the solution of large sparse linear systems of the general form

$$(J - \sigma I)\boldsymbol{x} = \boldsymbol{b} \tag{1}$$

with σ defining the shift and J as the fluid Jacobian matrix. We use an extension of the basic GCRO-DR iterative solver, referred to as GCRO-DR-R, which enables recycling of the invariant Krylov subspace not only during one linear solve, but also between consecutive solves (hence the final -R in the acronym). This is particularly convenient when used in conjunction with ARPACK since the coefficient matrix stays constant throughout, only depending on the applied fixed shift. Figure 9a shows typical convergence histories for different linear solvers just below buffet onset. Standard GMRES fails with a reasonable number of Krylov vectors, set 180 in this case to avoid excessive memory. The more advanced solver GCRO-DR with a Krylov basis of 180 and 20 restart vectors converges quickly following modest initial stagnation. The most impressive result is obtained using GCRO-DR-R which also recycles between solves with different right-hand sides. The

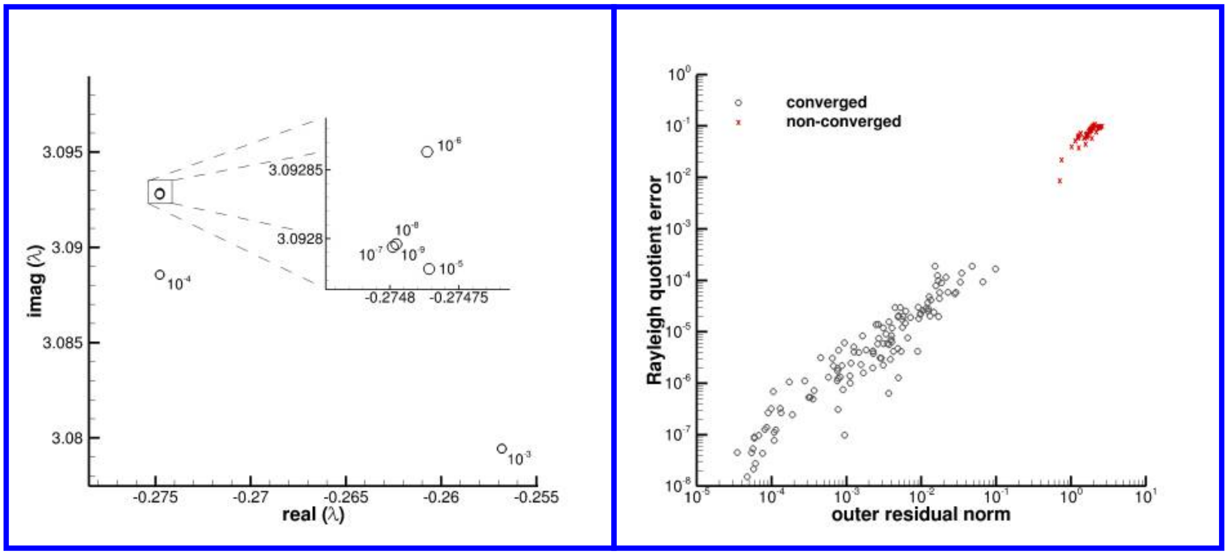

(a) convergence of eigenvalue with respect to inner convergence tolerance using shift $\sigma = 3.0i$

(b) relation between Rayleigh quotient error and outer residual norm

Figure 10. Converged and non-converged eigenvalues at angle of attack of 3.0 deg.

rate of convergence immediately follows the asymptotic behaviour of the basic solver offering an additional saving of factor 3. While the iterative solver is very robust, its performance depends on various factors including angle of attack, chosen shift, etc..

Since we are applying iterative solution methods, in contrast to previous work applying sparse direct solvers, the convergence behaviour of the inner-outer system needs to be investigated. The inner iteration refers to the solution of the linear system of equations given in Eq. (1) for each outer iteration, which on the other hand is given by a step of the implicitly restarted Arnoldi method. Figure 9b indicates a linear relationship between the inner convergence tolerance and the outer residual norm. The norm of the outer residual corresponds to the eigenvalue problem to be solved and is given by

$$\|J\boldsymbol{\phi}_f - \lambda\boldsymbol{\phi}_f\| \tag{2}$$

where $\boldsymbol{\phi}_f$ is the eigenvector of the fluid equations of unit norm and λ is the corresponding eigenvalue. To avoid the influence of the abort criterion in the implicitly restarted Arnoldi method, we simply set it to a number below the inner convergence tolerance. This parameter can be fine-tuned in future studies.

The corresponding convergence behaviour of one eigenvalue close to the complex-valued shift $\sigma = 3.0i$ is illustrated in Figure 10a. A quick convergence with respect to the inner convergence tolerance is observed. From an engineering point-of-view, not more than four to five order of magnitude inner convergence is required to have an accurate eigenvalue estimate. To check the quality of the computed eigenpairs, an additional criterion, besides the outer residual norm in Eq. (2), is applied.[28,29] The Rayleigh quotient error is the absolute value of the difference between the eigenvalue returned from ARPACK and the eigenvalue computed via the Rayleigh quotient from the corresponding eigenvector. It is given by the expression

$$|\lambda - \boldsymbol{\phi}_f^H J\boldsymbol{\phi}_f| \tag{3}$$

with superscript H indicating the conjugate transpose. Figure 10b presents all the eigenvalues, converged and non-converged, at 3.0 deg angle of attack for an entire sweep along the imaginary axis. The upper cloud of eigenvalues in the figure, located about two orders of magnitude above the converged bunch in terms of Rayleigh quotient error, corresponds to reduced-frequency shifts below one. These shifts are closest to the spectrum. As a remedy for such inconvenient numerical characteristics, shifts with positive damping are applied instead to increase the distance to the spectrum. The simulations then converged neatly.

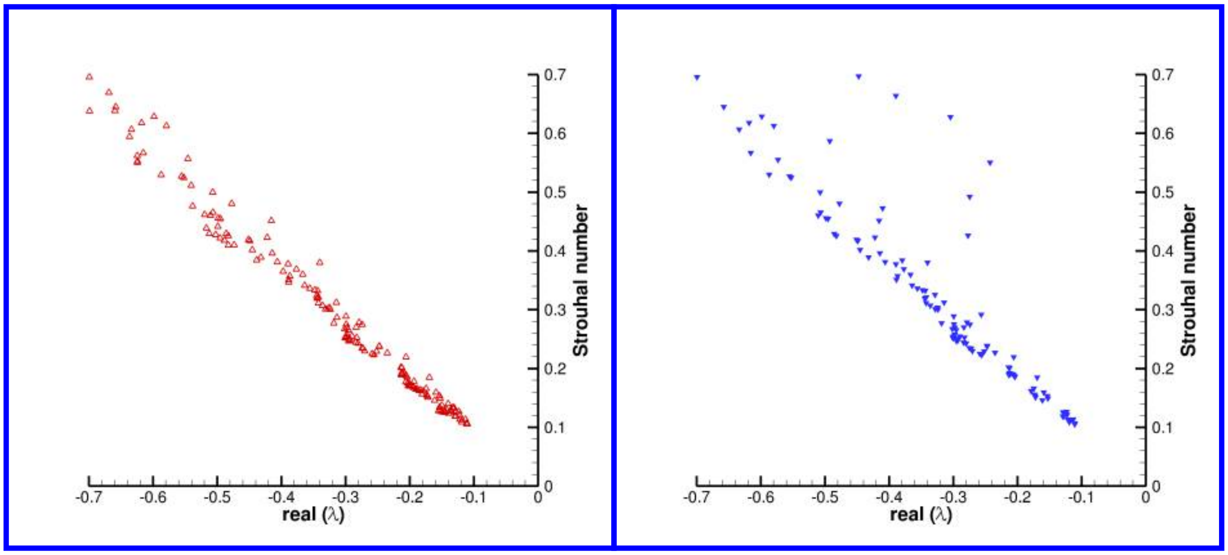

(a) eigenspectrum at 2.9 deg angle of attack

(b) eigenspectrum at 3.0 deg angle of attack

Figure 11. Eigenvalues of fluid Jacobian matrix on half wing-body configuration.

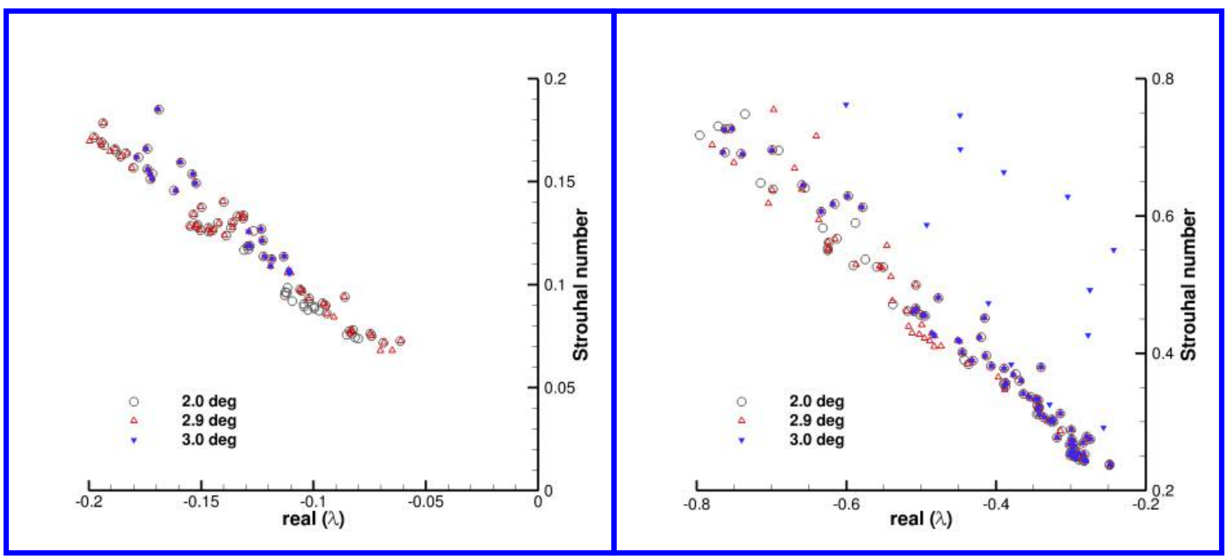

(a) lower frequency range

(b) upper frequency range

Figure 12. Eigenvalues of fluid Jacobian matrix on half wing-body configuration - close up view.

Figures 11 and 12 present the computed eigenvalues showing, for reasons of consistency, the Strouhal number over the eigenvalue's real part. Note that there are millions of eigenvalues and the methods presented, applying shifts along and close to the imaginary axis, are only capable to extract eigenvalues along the outskirts of the spectrum. This however is the region of immediate interest from a global-stability point of view. Moving the shift inside the spectrum to extract eigenvalues anywhere, while theoretically possible, would spiral up the computational cost considerably with limited gain in physical understanding. An overview of a part of the eigenspectrum is shown in Figure 11 for angles of attack of 2.9 and 3.0 deg. It is observed that for the higher angle of attack, a distinct group of eigenvalues with Strouhal numbers of about 0.3 to 0.7 emerges from the dense band to approach the imaginary axis. These distinct eigenvalues correspond to the emergence of the unusual higher-frequency behaviour observed in Figure 5 for forced-response calculations. Note that these solutions are properly converged following the criteria specified above. In particular, the norm of the outer residual vector (with a dimension of about 16.3 million) in Eq. (2) has a value between 10^{-4} and 10^{-5} throughout. Figure 12 gives more detail providing a close up view in the two Strouhal number regions of interest for angles of attack of 2.0, 2.9 and 3.0 deg. Additional simulation results are expected in the lower-frequency range to potentially link the resonance behaviour found from forced excitation with a destabilising global mode.

IV. Conclusions

The paper presents a numerical study of the flow over a representative half wing-body civil aircraft configuration. The focus is on the prediction of the onset of the transonic shock buffet instability. The shock buffet phenomenon involves transonic turbulent flow with strong unsteady shock waves and intermittent boundary layer separation. First, a forced-motion, time-linearised analysis is performed by exciting the wing structure using a sythetic torsion mode to investigate the frequency response behaviour of aerodynamic coefficients while approaching the buffet onset angle of attack. Secondly, global stability analysis with three inhomogeneous spatial directions is achieved on this realistic aircraft configuration with over 16 million unknowns. Here the implicitly restarted Arnoldi method is applied, in conjunction with an advanced sparse iterative linear equation solver and the industrial computational fluids dynamics package DLR-TAU, to calculate eigenvalues of the fluid Jacobian matrix.

Forced-response calculations reveal two interesting characteristics while approaching the instability. At lower frequencies results similar to forced-response calculations previously reported on two-dimensional aerofoils are observed. A distinct resonance peak combined with a phase lead of the aerodynamic coefficient with respect to the structural excitation is gradually formed when increasing the angle of attack. At higher frequencies, typical for three-dimensional shock buffet, an as yet unreported frequency response is found indicating the presence of destabilising global modes. The emergence of such destabilising global modes approaching the imaginary axis in the higher-frequency range is then confirmed by means of a global stability analysis extracting eigenvalues at several angles of attack in pre-buffet.

The lower-frequency behaviour following forced excitation, which would indicate a mechanism similar to buffet onset on aerofoils, has not yet been linked to the presence of a destabilising global mode. Further simulation results are expected to provide more conclusive data. In addition, different forms of excitation, besides a forced pitching structural motion, need to be analysed to understand why an imperfectly converged steady-state solution, used as initial disturbance for a time-marching simulation, only shows clear responses in the higher-frequency range.

References

[1] Reneaux, J., Brunet, V., Caruana, D., Deck, S., and Naudin, P., "A combined experimental and numerical investigation of the buffet phenomenon and its control through passive and active devices," Tech. Rep. Tiré à Part 2005-103, ONERA, 2005.

[2] Brunet, V. and Deck, S., "Zonal-detached eddy simulation of transonic buffet on a civil aircraft type configuration," *Advances in Hybrid RANS-LES Modelling*, Springer, 2008, pp. 182–191.

[3] Sartor, F. and Timme, S., "Reynolds–averaged Navier–Stokes simulations of shock buffet on half wing-body configuration," *AIAA Paper 2015–1939*, 2015.

[4] Sartor, F. and Timme, S., "Mach number effects on buffeting flow on a half wing body configuration," *50th 3AF International Conference on Applied Aerodynamics*, 2015.

[5] Crouch, J. D., Garbaruk, A., and Magidov, D., "Predicting the onset of flow unsteadiness based on global instability," *Journal of Computational Physics*, Vol. 224, No. 2, 2007, pp. 924–940.

[6] Crouch, J. D., Garbaruk, A., Magidov, D., and Travin, A., "Origin of transonic buffet on aerofoils," *Journal of Fluid Mechanics*, Vol. 628, 2009.

[7] Sartor, F., Mettot, C., and Sipp, D., "Stability, receptivity and sensitivity analyses of buffeting transonic flow over a profile," *AIAA Journal*, Vol. 53, No. 7, 2015, pp. 1980–1993.

[8] Iorio, M. C., Gonzalez, L. M., and Ferrer, E., "Direct and adjoint global stability analysis of turbulent transonic flows over a NACA0012 profile," *International Journal for Numerical Methods in Fluids*, 2014, pp. 147–168.

[9] Elman, H. C., Meerbergen, K., Spence, A., and Wu, M., "Lyapunov inverse iteration for identifying Hopf bifurcations in models of incompressible flow," *SIAM Journal on Scientific Computing*, Vol. 34, No. 3, 2012, pp. A1584–A1606.

[10]Timme, S., Badcock, K. J., Wu, M., and Spence, A., "Lyapunov inverse iteration for stability analysis using computational fluid dynamics," *AIAA Paper 2012-1563*, 2012.

[11]Lehoucq, R. B., Sorensen, D. C., and Yang, C., *ARPACK Users' Guide: solution of large-scale eigenvalue problems with implicitly restarted Arnoldi methods*, SIAM, 1998.

[12]Maschhoff, K. J. and C.Sorensen, D., "P_ARPACK: An efficient portable large scale eigenvalue package for distributed memory parallel architectures," *Lecture Notes in Computer Science*, Vol. 1184, 1996, pp. 478–486.

[13]Saad, Y. and Schultz, M. H., "GMRES: A Generalized Minimal Residual Algorithm for Solving Nonsymmetric Linear Systems," *SIAM J. Sci. Stat. Comput.*, Vol. 7, No. 3, 1986, pp. 856–869.

[14]Lawson, S., Greenwell, D., and Quinn, M. K., "Characterisation of Buffet on a Civil Aircraft Wing," *AIAA 2016-1309*, 2016.

[15]Martineau, D. G., Stokes, S., Munday, S. J., Jackson, A. P., Gribben, B. J., and Verhoeven, N., "Anisotropic hybrid mesh generation for industrial RANS applications," *AIAA Paper 2006-534*, 2006.

[16]Allmaras, S. R., Johnson, F. T., and Spalart, P. R., "Modifications and clarifications for the implementation of the Spalart–Allmaras turbulence model," *ICCFD7-1902*, 2012.

[17]Xu, S., Timme, S., and Badcock, K. J., "Krylov subspace recycling for linearised aerodynamics analysis using DLR-TAU," *International Forum on Aeroelasticity and Structural Dynamics, IFASD 2015-186*, 2015.

[18]McCracken, A., Da Ronch, A., Timme, S., and Badcock, K. J., "Solution of linear systems in Fourier-based methods for aircraft applications," *International Journal of Computational Fluid Dynamics*, Vol. 27, No. 2, 2013, pp. 79–87.

[19]Thormann, R. and Widhalm, M., "Linear-frequency-domain predictions of dynamic-response data for viscous transonic flows," *AIAA Journal*, Vol. 51, No. 11, 2013, pp. 2540–2557.

[20]Bekemeyer, P. and Timme, S., "Reduced order gust response simulation using computational fluid dynamics," *AIAA-2016-1485*, 2016.

[21]Dandois, J., "Experimental study of transonic buffet phenomenon on a 3D swept wing," *Physics of Fluids*, Vol. 28, No. 1, 2016.

[22]Nitzsche, J., "A numerical study on aerodynamic resonance in transonic separated flow," *International Forum on Aeroelasticity and Structural Dynamics, IFASD 2009-126*, 2009.

[23]Iovnovich, M. and Raveh, D. E., "Transonic unsteady aerodynamics in the vicinity of shock-buffet instability," *Journal of Fluids and Structures*, Vol. 29, 2012, pp. 131–142.

[24]Thormann, R., Nitzsche, J., and Widhalm, M., "Time-linearized simulation of unsteady transonic flows with shock-induced separation," *6th European Congress on Computational Methods in Applied Sciences and Engineering*, 2012.

[25]Li, X. S., "An overview of SuperLU: algorithms, implementation, and user interface," *ACM Transactions on Mathematical Softwaretoms*, Vol. 31, No. 3, September 2005, pp. 302–325.

[26]Amestoy, P. R., Duff, I. S., L'Excellent, J.-Y., and Koster, J., "A fully asynchronous multifrontal solver using distributed dynamic scheduling," *SIAM Journal on Matrix Analysis and Applications*, Vol. 23, No. 1, 2001, pp. 15–41.

[27]Thormann, R. and Timme, S., "Efficient aerodynamic derivative calculation in three-dimensional transonic flow," *Royal Aeronautical Society 2016 Applied Aerodynamics Conference*, 2016.

[28]Burroughs, E. A., Romero, L. A., Lehoucq, R. B., and Salinger, A. G., "Large scale eigenvalue calculations for computing the stability of buoyancy driven flows," Tech. Rep. SAND2001-0113, Sandia National Laboratories, 2001.

[29]Burroughs, E. A., Romero, L. A., Lehoucq, R. B., and Salinger, A. G., "Linear stability of flow in a differentially heated cavity via largescale eigenvalue calculations," *International Journal of Numerical Methods for Heat & Fluid Flow*, Vol. 14, No. 6, 2004, pp. 803–822.